

Contents lists available at ScienceDirect

Physica D

journal homepage: www.elsevier.com/locate/physd



Dispersive shock waves in lattices: A dimension reduction approach

Check for updates

Christopher Chong a,*, Michael Herrmann b, P.G. Kevrekidis c

- ^a Department of Mathematics, Bowdoin College, Brunswick, ME 04011, United States of America
- ^b Institute of Partial Differential Equations, Technische Universität Braunschweig, 38106 Braunschweig, Germany
- ^c Department of Mathematics and Statistics, University of Massachusetts Amherst, Amherst, MA 01003-4515, United States of America

ARTICLE INFO

Article history: Received 22 June 2022 Received in revised form 13 September 2022 Accepted 16 September 2022 Available online 26 September 2022 Communicated by B.-F Feng

Keywords: Dispersive shock waves Nonlinear lattice Discrete conservation law

ABSTRACT

Dispersive shock waves (DSWs), which connect states of different amplitude via a modulated wave train, form generically in nonlinear dispersive media subjected to abrupt changes in state. The primary tool for the analytical study of DSWs is Whitham's modulation theory. While this framework has been successfully employed in many space-continuous settings to describe DSWs, the Whitham modulation equations are cumbersome in most spatially discrete systems. In this article, we illustrate the relevance of the reduction of the DSW dynamics to a planar ODE in a broad class of lattice examples. Solutions of this low-dimensional ODE accurately describe the orbits of the DSW in self-similar coordinates and the local averages in a manner consistent with the modulation equations. We use data-driven and quasicontinuum approaches within the context of a discrete system of conservation laws to demonstrate how the underlying low dimensional structure of DSWs can be identified and analyzed. The connection of these results to Whitham modulation theory is also discussed.

© 2022 Elsevier B.V. All rights reserved.

1. Introduction

Understanding how systems respond to sudden changes in the medium is critical in a number of applications. Classic examples include explosions in shock tubes [1], when gases or fluids are compressed in a piston chamber [2] or when water dams break [3]. From a modeling perspective, a sudden change in a medium is often represented by step initial data (the so-called Riemann problem). In mathematical models describing fluid or gas dynamics based on space and time continuous conservation laws, states of different amplitude that are connected via a discontinuity (i.e., fronts involving jumps, e.g., in density or concentration) are predicted to travel through the medium at constant speed and are called Lax shock waves [4], or just shocks. Since solutions with infinite derivatives are nonphysical, modified (e.g., regularized) models are often used as an alternative. In some settings, such as stratified environments of the ocean and atmosphere, dispersive shocks (and their regularizations) are more relevant [5,6]. In this case, the states of different amplitude are connected via an expanding modulated wave train. This structure is called a dispersive shock wave (DSW). The primary tool to analytically describe DSWs is Whitham's modulation theory [7-9]. In this framework, one derives equations describing slow modulations of the underlying parameters of a periodic wave

E-mail address: cchong@bowdoin.edu (C. Chong).

by, for example, averaging the Lagrangian action integral over a family of periodic wave trains [10,11].

The study of DSWs in spatially continuous media has been ongoing since Whitham's seminal work [7] over 50 years ago, but there has been renewed excitement for this theme. This excitement has largely been inspired by recent groundbreaking experimental observations of DSWs most notably in ultracold gases and superfluids [12,13], nonlinear optics [14,15], and fluid conduits [5,16], among others. Dispersive shock waves in onedimensional (1D) nonlinear lattices (to be called lattice DSWs) have been explored numerically, and even experimentally in several works [17-23]. Although much of the above motivation in discrete systems stems from the material science of granular crystals, it is of broad physical interest, as similar structures have been experimentally observed, e.g., in nonlinear optics of waveguide arrays [24]. The existence of periodic waves has been proved [25-27] and corresponding modulation equations have been derived [28,29]. Explicit forms of the periodic waves are typically not available, resulting in modulation equations that are rather cumbersome (and, plausibly for this reason, have not been much studied to date). Even in the integrable paradigm of the Toda lattice, the modulation equations are quite cumbersome [30-32]. This is one reason the mathematical theory of lattice DSWs is not as mature when compared to the study of DSWs in continuous settings, which has seen many recent experimental and theoretical advancements, as summarized in the reviews [10,11,33].

^{*} Corresponding author.

A first goal of this paper is to provide a complementary approach to modulation theory for the description of lattice DSWs in a broad class of nonlinear lattice dynamical models. Subsequently, we aim to unveil the crucial observation that lattice DSW dynamics can be reduced to a planar ODE which can be handled analytically. After detailing the problem set-up in Section 2, we explore two approaches towards identifying the underlying ODE dynamics: a data driven one in Section 3 and one based on a quasi-continuum approximation in Section 4. The obtained results are discussed within the context of the modulation equations in Section 5. Section 6 concludes the paper. We believe that the method presented herein offers a key insight of relevance to a wide class of lattice models bearing DSWs and the method of analysis offers a quantitative perspective on the DSW dynamics that is found to be in good agreement with the numerical observations in suitable regimes of the wave speed c. A discussion of the modulation equations in terms of the wave parameters is discussed in further detail in Appendix A.

2. Model equations and problem statement

In order to explore lattice DSWs and the dimensionality reduction approach, the following wide class of nonlinear dynamical lattices is considered [34]

$$2\frac{du_n}{dt} + \Phi'(u_{n+1}) - \Phi'(u_{n-1}) = 0, (1)$$

where $n \in \mathbb{Z}$, $t \in \mathbb{R}$, $u = u_n(t) \in \mathbb{R}$ and the potential $\Phi(u)$ is assumed to be convex. Eq. (1) possesses a Lagrangian and Hamiltonian structure [35], yet it is first order only, making its analysis slightly more convenient when compared to classical nonlinear oscillators, such as those of the Fermi-Pasta-Ulam-Tsingou (FPUT) type [36]. We expect that the reduction approach that is presented here will be applicable to a large class of lattice systems, such as FPUT models [37], discrete Nonlinear Schrödinger models [38], and discrete Klein Gordon models [39]. Besides serving as a prototype model for lattice DSWs, Eq. (1) is also directly relevant for applications, such as in the description of traffic flow [40]; for a discussion of relevant models and their continuum limits see also Ref. [34]. Eq. (1) is a centered difference scheme for the space and time continuous conservation law

$$\partial_T U + \partial_X \Phi'(U) = 0, \tag{2}$$

where $X, T \in \mathbb{R}$, $U = U(X, T) \in \mathbb{R}$, and the discrete and continuous variable are related through $u_n(t) = U(\varepsilon n, \varepsilon t) = U(X, T)$ with $0 < \varepsilon \ll 1$. It is well known that Lax shocks can form in Eq. (2) subjected to Riemann initial data for a large class of flux functions Φ' [4]. Eq. (1) can be thought of as a dispersive regularization of Eq. (2) [41], and hence, it is expected that dispersive shock waves will form when subjected to Riemann initial data instead of Lax shocks [34].

For demonstration purposes, we will primarily consider the polynomial potential

$$\Phi(u) = \frac{u^2}{2} + \frac{u^4}{4},\tag{3}$$

although, we also present results for the Kac-van-Moerbeke (KvM) potential, $\Phi(u) = \exp(u)$, to demonstrate the generality of the presented approach. Note that Eq. (1) with the KvM potential is completely integrable [40,42] although this fact will play no role in the analysis, as the methods presented below are of interest more broadly to dispersive nonlinear lattice systems (rather than more restrictively integrable ones).

Throughout the manuscript we consider Riemann (i.e. step) initial data,

$$u_n(0) = \begin{cases} 1, & n \le 0 \\ 0, & n > 0 \end{cases} \tag{4}$$

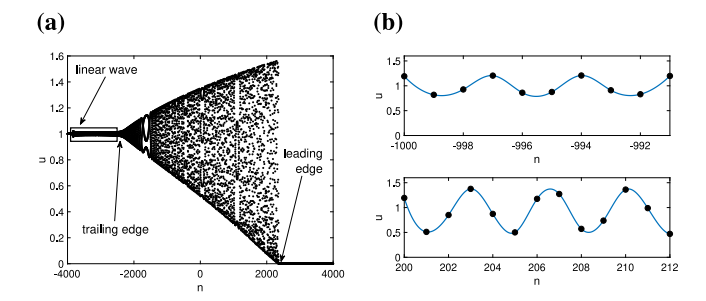


Fig. 1. (a) Example of lattice DSW. Result obtained via numerical simulation of Eq. (1) with N=8000 and the polynomial potential, Eq. (3), starting from Riemann initial data, Eq. (4). The solution at t=960 is shown. The box labeled "linear wave" vanishes in the large lattice limit. **(b)** Zoom of panel (a) at near n=-1000 (top) and n=200 (bottom). The solid lines are the interpolating splines, shown for visual clarity. The profiles resemble periodic waves, albeit with different parameters, in each zoom.

to generate DSWs. Letting N (even) represent the number of spatial points, we define $\varepsilon = 1/N$. The corresponding spatial domain is $-N/2 + 1 < n \le N/2$ and the temporal domain is $[0, T_f/\varepsilon]$, where T_f is a fixed constant independent of ε . One example of a DSW that has formed starting with (4) is shown in Fig. 1(a). For every finite lattice, there is a linear wave centered at unity (see boxed area in Fig. 1(a)), which vanishes according to the decay law $\sim N^{-1/3}$ [43]. The trailing edge of the DSW can be described in the zero amplitude, harmonic wave limit. In this limit it is found that the trailing edge speed is consistent with the local linear group velocity. At the leading edge of the DSW (e.g. in the zero-wavenumber limit) the profile is close to a solitary wave solution. The leading and trailing edges of the DSW are discussed in greater detail in Appendix B. The structure of the DSW away from these two limiting cases is less apparent. To better understand the interior of the DSW, notice that the trajectory of the DSW in each small window of space and time appears to be a traveling periodic wave, see Fig. 1(b). The existence of traveling periodic waves of Eq. (1) was established in Ref. [35]. They have the form

$$u_n(t) = V + \mathcal{V}(\zeta), \qquad \zeta = Kn - \Omega t,$$
 (5)

where the parameters V (mean), K (wave vector) and Ω (frequency) are real and the wave profile V is assumed, w.l.o.g, to be 2π periodic with mean zero. By substituting Eq. (5) into Eq. (1), one finds that V must satisfy the advance-delay equation,

$$2\Omega \mathcal{V}'(\zeta) = \Phi'(V + \mathcal{V}(\zeta + K)) - \Phi'(V + \mathcal{V}(\zeta - K)). \tag{6}$$

Within the "core" of the DSW (i.e., the modulated wave connecting the two constant states), the wave parameters, V, K and Ω appear to be different in each small spatiotemporal window (compare the top and bottom panels of Fig. 1(b)). This suggests that a DSW can be viewed as a traveling periodic wave with slowly varying parameters that connect the left state $u_{-}=1$ to the right state $u_+ = 0$. The set of equations that describe how the wave parameters, V, K and Ω vary within the core of the DSW is referred to as the system of modulation equations (relevant details are given in Section 5 and Appendix A). There is no explicit form for the traveling wave profile \mathcal{V} for general potentials $\Phi(u)$, which satisfies the above advance-delay differential Eq. (6). This results in modulation equations that are fairly cumbersome in the discrete setting. Thus, in order to obtain a useful analytical description of a lattice DSW, an approach that is complementary to the modulation theory seems necessary. We now discuss such an approach.

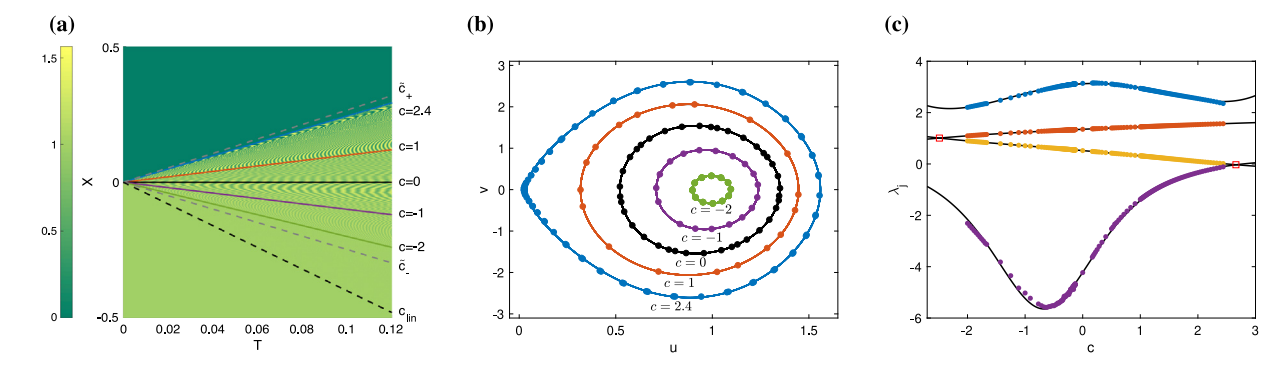


Fig. 2. (a) Intensity plot of a lattice DSW (same parameters as in Fig. 1) with axes corresponding to the slow variables $X = \varepsilon n$ and $T = \varepsilon t$. Color intensity corresponds to amplitude (see colorbar). Each solid line corresponds to a fixed value of the self-similar speed c = X/T. The dashed lines marked \tilde{c}_+ and \tilde{c}_- are estimates of the leading and trailing edge of the DSW, respectively. The dashed line marked c_{lin} is the edge of the linear wave (see boxed area of Fig. 1(a)). The vertical slice at the final time shown (T = 0.12) corresponds to the profile in Fig. 1(a). (b) Phase plane of the data extracted along the lines c = X/T of the lattice DSW shown in panel (a) (markers), where $v = \dot{u}$. The solid lines are the planar ODE prediction of Eq. (9). (c) Plot of the roots (markers) of P(c). The roots are ordered by size: λ_1 (purple) $\leq \lambda_2$ (yellow) $\leq \lambda_3$ (red) $\leq \lambda_4$ (blue). Solid lines are the result of fitting the roots to a trial function of c; see relevant details in the text.

3. A planar ODE description of a lattice DSW

Fig. 2(a) shows an intensity plot of a numerical solution of Eq. (1) with initial data given by Eq. (4) and $\Phi(u) = \frac{u^2}{2} + \frac{u^4}{4}$ and N = 8000. A symplectic integrator is used for the direct simulation of Eq. (1), see [35]. Viewing the solution along slices of fixed t yields the usual DSW spatial profile, see Fig. 1(a). However, if one observes data along the DSW with n/t = X/T = c fixed, a nested, non-intersecting set of closed loops in the phase plane (u, \dot{u}) is formed, with each value of c representing a different loop, see Fig. 2(b). The fact that closed loops form is unsurprising, since it is expected that the DSW has a self similar structure, and hence, with X/T = c fixed, the modulation parameters should be fixed. What is surprising is that the set of loops is nested and non-intersecting when projecting the dynamics onto a two-dimensional phase space. This motivates the proposal to identify a planar ODE that can approximate the lattice DSW dynamics.

To identify such an ODE, we first take a data-driven approach. For each fixed value of c, we extract position and velocity data from the DSW. We define this data as $u=u_{ct}(t;c)$, where $u_{ct}(t;c)$ is the position data at lattice location n=ct and time t, which ensures that c=n/t. This necessitates that the time increment is chosen such that ct is an integer. Similarly, we define $v=v_{ct}(t;c)$, where $v_n=\dot{u}_n$. We assume there is a simple energy relationship between the position u and velocity v as follows

$$\frac{v^2}{2} = \sum_{i=0}^{M} v_i u^i(t;c) =: P(u;c).$$
 (7)

Treating u and v as independent and dependent variables, respectively, we determine the parameters v_i via a linear regression. This relationship will describe the periodic orbit making up the DSW at a particular value of the speed c. In order to extract the underlying structure of the entire DSW, we repeat the process for several c values that lie within the core of the DSW. For each value of c, we express the polynomial P in terms of its roots $P(u; c) = \Lambda(c)(u - \lambda_1(c))(u - \lambda_2(c))(u - \lambda_3(c))(u - \lambda_4(c))$ where the roots are ordered $\lambda_1 \leq \lambda_2 \leq \lambda_3 \leq \lambda_4$. The roots plotted against the speed c are the markers shown in Fig. 2(c). Once the roots and constant (i.e., u-independent) factor Λ are obtained, they are fitted to a simple trial function of c. How exactly the roots depend on c is critical in identifying the character of the DSW. This step of the process is similar to solving the modulation equations with boundary and initial data consistent with a DSW [8]. In particular, it is only though a very specific dependence of the roots on the parameter c that a DSW will arise. For the purpose of simplicity, polynomial trial functions are assumed, which capture the data

well (e.g., compare the lines and markers of the top three curves of Fig. 2(c)). The only exception to this choice of trial function was for the first root, λ_1 , in the case of the polynomial potential. This root is bell-shaped (see bottom curve Fig. 2(c)), and thus, the polynomial trial function led to a poor fit. Thus, a trial function in the form of a hyperbolic secant is used in this case. All other cases led to good agreement between the roots and a polynomial trial function. Note that the choice of trial function has no direct consequence on the forthcoming analysis. Upon performing the fitting, the resulting formulas are $\lambda_1(c) = -5.79 \text{sech}(-1.16(c+0.67)) + 0.20$, $\lambda_2(c) = -0.01c^2 - 0.20c + 0.52$, $\lambda_3(c) = -0.01c^2 + 0.10c + 1.35$, $\lambda_4(c) = 0.02c^3 - 0.19c^2 + 0.05c + 3.08$ and $\Lambda(c) = 0.40c^2 + 0.42c + 0.62$. Repeating the entire procedure for the KvM potential $\Phi(u) = \exp(u)$ leads to the formulas $\lambda_1(c) = 0.03c^3 - 0.42c^2 + 1.74c - 2.08$ (notice that in this case, a polynomial was used instead), $\lambda_2(c) = 0.01c^3 - 0.01c^2 - 0.38c + 0.72$, $\lambda_3(c) = -0.01c^3 - 0.02c^2 + 0.29c + 1.24$, $\lambda_4(c) = 0.04c^3 - 0.23c^2 + 0.06c + 3.43$ and $\Lambda(c) = 0.13c^2 + 0.25c + 0.49$.

Eq. (7) implies the following planar ODE is satisfied

$$\frac{d^2u}{d\tau^2} = P'(u; c), \quad u(0) = \lambda_2(c), \quad \frac{du}{d\tau} \bigg|_{\tau=0} = 0, \tag{8}$$

with $\tau \in [0, \tau_p]$ where τ_p is the period of oscillation and τ is related to the lattice time variable through the scaling $\tau = \alpha t$. While the time scaling factor is not needed for the forthcoming analysis, it can be approximated through the relation $\alpha = \tau_p/(T_p)$, where T_p is the period of oscillation of the DSW trajectory with c fixed. Note that both τ_p and T_p (and hence α) depend on c. Clearly, periodic waves of Eq. (8) will correspond to oscillations of u between roots of P(u;c) when P>0, such as $\lambda_2(c)$ and $\lambda_3(c)$. With the choice of initial values these extreme values occur for t=0 and $t=\tau_p/2$ such that $u(0)=\lambda_2$ is the minimum value and $u(\tau_p/2)=\lambda_3$ is the maximum. The period of oscillation is given by $\tau_p=2\int_0^{\tau_p/2} d\tau=2\int_{\lambda_2}^{\lambda_3} 1/\sqrt{2P(u)}\,du$. For the choice of the energy relationship given by Eq. (7), Eq. (8) can be solved using quadrature [44]. The exact solution is

$$u(\tau) = \frac{\lambda_2(\lambda_3 - \lambda_1) + \lambda_1(\lambda_2 - \lambda_3)\operatorname{sn}^2(\theta\tau; m)}{\lambda_3 - \lambda_1 + (\lambda_2 - \lambda_3)\operatorname{sn}^2(\theta\tau; m)},$$
(9)

where sn is a Jacobi elliptic function with parameter 0 < m < 1 and.

$$\theta = \sqrt{\frac{\Lambda(\lambda_3 - \lambda_1)(\lambda_4 - \lambda_2)}{2}}, \qquad m = \frac{(\lambda_3 - \lambda_2)(\lambda_4 - \lambda_1)}{(\lambda_3 - \lambda_1)(\lambda_4 - \lambda_2)}.$$

The periodic wave given by Eq. (9) has the period $\tau_p = 2K(m)/\theta$, where K(m) is the complete elliptic integral of the first kind.

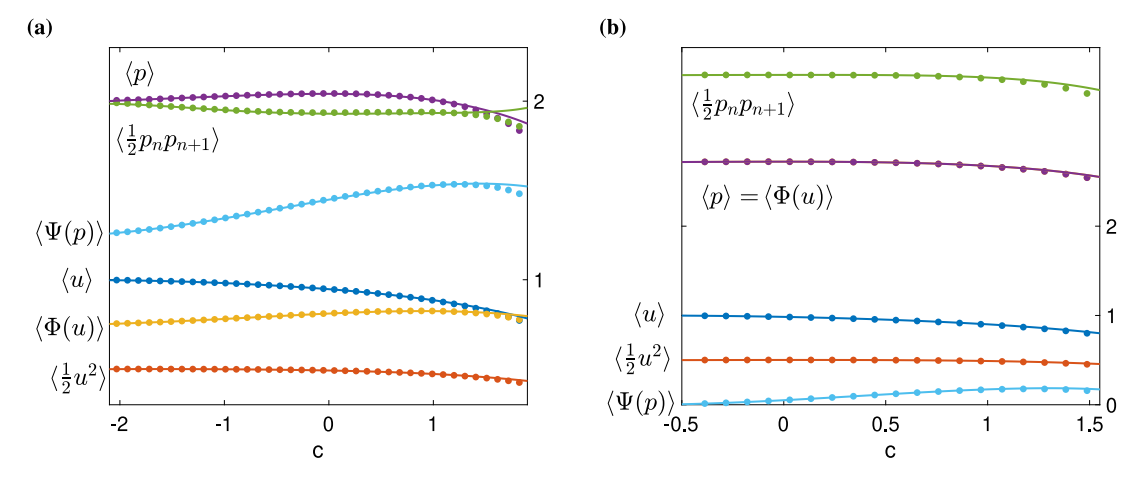


Fig. 3. (a) Local averages measured from the lattice DSW (markers) and the ODE prediction from Eq. (9) (solid curves) for the polynomial potential $\Phi(u) = u^2/2 + u^4/4$. (b): Same as panel (a) for the KvM potential $\Phi(u) = \exp(u)$.

Eq. (9) yields good agreement with the trajectories of the full lattice DSW dynamics, despite the simple choice of a polynomial for the energy relationship given by Eq. (7), (compare the lines and markers of Fig. 2(b)). Notice for $\lambda_1 \rightarrow \lambda_2$ we have $m \rightarrow 1$, and thus, the period tends to infinity and the solution tends to a homoclinic connection. This limit corresponds to the leading edge of the DSW. For the polynomial potential, the ODE prediction is $\tilde{c}_{+}=2.66$, which overestimates the observed value of $c_{+}=2.45$. For $\lambda_3 \to \lambda_2$ we have $m \to 0$, in which case the solution tends to a constant. This is the trailing edge of the DSW, which is predicted by the ODE to occur for $\tilde{c}_- = -2.48$, which is quite close to the value extracted from the full lattice DSW $c_{-}=-2.50$. See the red boxes of Fig. 2(c) showing where the roots coalesce and the gray dashed lines of Fig. 2(a) for a comparison of the predicted and actual DSW edges. For the KvM potential, the trailing and leading edge extracted from the lattice DSW are $c_{-} = -0.71$ and $c_{+}=1.98$, and the ODE predictions are $\tilde{c}_{-}=-0.73$ and $\tilde{c}_{+} = 2.10.$

3.1. ODE prediction of local averages

There are various quantities that can be used to identify the character of a DSW. One is the spatial profile, as shown in Fig. 1. For larger lattice sizes, however, the structure can be difficult to analyze when viewing the DSW in this way. Another possibility is to inspect local averages, which can be computed directly from the lattice DSW data and from our ODE prediction. The local averages we consider are $\langle u_n \rangle$, $\langle p_n \rangle$, $\langle \Phi(u_n) \rangle$, $\langle p_n p_{n+1}/2 \rangle$, $\langle u_n^2/2 \rangle$ and $\langle \Psi(p) \rangle$ where the angle brackets denote the local average with respect to the traveling wave coordinate, the dual variable is $p = \Phi'(u)$ and $\Psi(p) = pu - \Phi(u)$ is the Legendre transform of $\Phi(u)$. The reason we investigate these specific choices of local averages is their connection to the modulation equations (see discussion in Section 5). Thus, we can bridge results based on the standard modulation theory approach and our proposed ODE reduction approach.

Note that the local averages are, in principle, expressible in terms of the traveling wave parameters V, K and Ω . For example,

$$\langle u \rangle := \frac{1}{2\pi} \int_0^{2\pi} V + \mathcal{V}(\zeta) \, d\zeta = V,$$

where ζ is the traveling wave coordinate. The other local averages cannot be evaluated explicitly in general, however, since the periodic wave profile $\mathcal V$ is defined implicitly by an advance-delay equation, in which there is no closed-form solution. We estimate

the local averages numerically from the DSW data as a function of c=n/t as follows

$$\langle u \rangle \approx \frac{1}{T_p} \int_{n/c}^{n/c+T_p} \frac{1}{2N} \sum_{m=n-N}^{n+N} u_m(t) dt.$$
 (10)

where the sum appearing in the integrand is a mesoscopic average where $\mathcal N$ is chosen to be larger than the spatial wavelength but much smaller than the lattice size. We chose $\mathcal N=300$. The use of the mesoscopic spatial average leads to smoother data (e.g. the oscillations are effectively averaged out), but the data close to the boundaries will not have estimates for the averages. Similar computations are made for the remaining five local averages (see the markers of Fig. 3).

We will now compute local averages directly from the planar ODE solution of Eq. (9). For example,

$$\langle u \rangle = \lambda_1 + \frac{\lambda_2 - \lambda_1}{4K(m)} \Pi\left(\frac{\lambda_3 - \lambda_1}{\lambda_3 - \lambda_2}, m\right),$$
 (11)

where $\Pi(C; m)$ is the complete integral of the third kind with elliptic characteristic C, and parameter m. The remaining five local averages can also be expressed in terms of elliptic integrals (see the solid lines of Fig. 3).

The analytical predictions for the local averages based on the planar ODE are very close to the local averages computed directly from the lattice DSW for the polynomial potential and the KvM potential (compare the lines and markers of Fig. 3). The analytical local averages provide a layer of insight that is not available using the numerically obtained averages. We were able to obtain the formulas leveraging our data-driven approach, and without the need to derive or solve a set of cumbersome modulation equations.

4. Quasi-continuum approximation

4.1. A straightforward continuum limit

Having demonstrated that there is an underlying low-dimensional ODE structure to a lattice DSW, it is reasonable to ask where this ODE structure comes from. While there are possibly many ways in which this structure could manifest, a natural one to consider is the large lattice nature of the problem (in this article N=8000). We now investigate this possibility by taking a suitable continuum limit of the lattice dynamics (bearing a leading order lattice-induced correction). This approach has been used to study DSWs in FPUT type lattices [45,46] and will

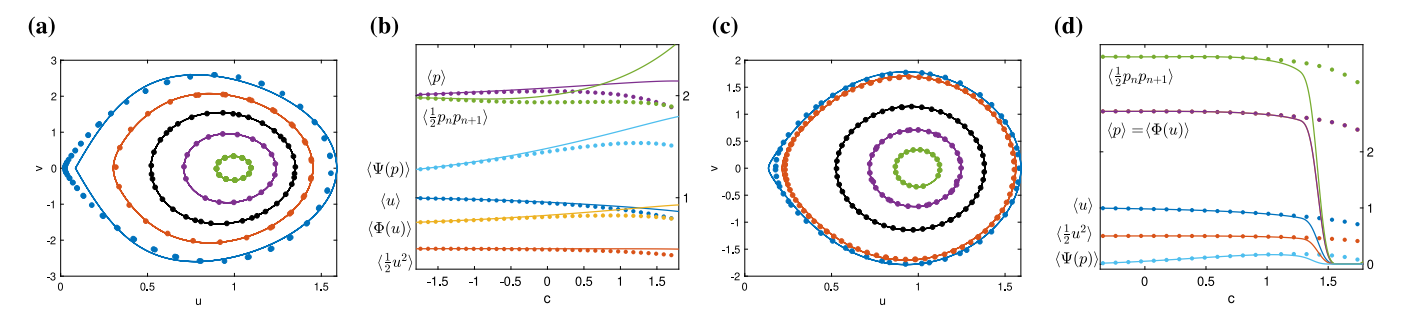


Fig. 4. (a) Phase plane of the data extracted along the lines c = X/T of a lattice DSW for the polynomial potential (markers), see also Fig. 2(b). The solid lines are the planar ODE prediction of Eq. (8) using the energy relationship given by Eq. (14) (i.e., the quasi-continuum approximation). **(b)** Local averages measured from the lattice DSW (markers) and the ODE prediction based on the quasi-continuum approximation. **(c,d)** Same as panel (a) and (b), respectively, for the KvM potential.

be useful here as well. Using the hyperbolic scaling $u_n(t) = U(\varepsilon n, \varepsilon t) = U(X, T)$ the discrete conservation law Eq. (1) can be approximated by the following quasi-continuum model

$$\partial_T U = -\left(\partial_X + \frac{\varepsilon^2}{6}\partial_X^3\right) \Phi'(U),\tag{12}$$

which is the same as Eq. (2) with the next order term in the expansion kept. Indeed, Eq. (12) can be thought of as a dispersive regularization of Eq. (2). Notice that the small parameter ε appears explicitly in the model equation, making the error hard to control. This is why Eq. (12) is called a guasi-continuum model rather than a continuum model. Uncontrollable errors are typical in quasi-continuum models, see the discussion in [47], which is in contrast to continuum models derived from other scalings, such as the Korteweg-de Vries or Nonlinear Schrödinger scalings, which have controllable errors [48]. Indeed, similar quasicontinuum models derived, for example, in the context of FPUT lattices have both failed and succeeded in representing the actual lattice dynamics (see the discussion in [49,50]). Thus, it is important to check directly the validity of a PDE such as Eq. (12). Here, we will do so at the (reduced) level of the effective planar ODE description. To that effect, we first move into the co-traveling frame via the traveling wave ansatz $U(X,T) = \phi(KX - \Omega T) =$ $\phi(\zeta)$. Substitution of this expression into Eq. (12) and integrating once leads to

$$-\Omega\phi + \left(K + \frac{\varepsilon^2 K^3}{6} \frac{d^2}{d\zeta^2}\right) \Phi'(\phi) + A = 0, \tag{13}$$

where *A* is an arbitrary integration constant. This equation has the following conserved quantity

$$E(\phi, v) = \frac{K^3 \varepsilon^2}{6} \frac{(\Phi''(\phi)v)^2}{2} + \int (K\Phi'(\phi) - \Omega\phi + A)\Phi''(\phi) d\phi.$$

If the planar structure identified in Fig. 2(b) was a direct result of the large lattice size, the trial form of the energy should be,

$$\frac{v^2}{2} = \frac{6}{\varepsilon^2 K^3} \frac{E - \int (K\Phi'(\phi) - \Omega\phi + A)\Phi''(\phi) d\phi}{\Phi''(\phi)^2}.$$
 (14)

Using the functional form of Eq. (14), we find best-fit values of the parameters E, K, Ω , A as functions of c. The reduced ODE once again has the form given by Eq. (8), but with P being replaced by the right-hand-side of Eq. (14). Solutions of this reduced ODE (computed numerically in this case) compare somewhat reasonably to the full lattice dynamics, see Fig. 4(a,c). In this case, the deviation between the actual lattice DSW and the ODE solution becomes larger as the leading edge of the DSW is approached (see the outermost orbit of Fig. 4(a), for example). The difference between the ODE prediction and lattice DSW becomes even more apparent when inspecting the local averages, where the deviation can become significant for models with the polynomial potential and the KvM potential, see Fig. 4(b,d). In the case of the KvM

potential, one notable difference when using Eq. (14) instead of Eq. (7) is that the leading edge is predicted to occur for a smaller value of c. In particular the predicted leading edge is $\tilde{c}_+ \approx 1.5$ where the observed leading edge is $c_+ \approx 1.98$. This explains the steep decay of the local averages for $c \approx 1.5$ in Fig. 4(d). In both cases, it is clear that the ODE prediction based on the quasi-continuum energy relationship yields poorer results than those using the data-driven polynomial energy relationship. Nevertheless, the relevant prediction is quite adequate for sufficiently small values of c and provides a good qualitatively and even reasonable semi-quantatively representation of the corresponding phase portrait in Fig. 4 (see panels (a) and (c)), with a theoretical foundation stemming from the underlying lattice dynamics. Before moving on, we briefly investigate an alternative quasi-continuum model.

4.2. The Rosenau regularization

Quasi-continuum models derived in the fashion detailed above often have the unfortunate side affect of being ill-posed due to large wavenumber instabilities in the associated dispersion relation [51–53]. In [54,55] (see also the discussion in [18]). Rosenau proposed a regularization of such models to avoid the issue of ill-posedness. We will use the same regularization in order to obtain an alternate quasi-continuum model. The regularized model is obtained by inverting the operator $(1+\frac{\varepsilon^2}{6}\partial_\chi^2)$ in Eq. (12) and Taylor expanding it (on the left-hand side of the equation), which leads to

$$\partial_T U = -\partial_X \Phi'(U) + \frac{\varepsilon^2}{6} \partial_X^2 \partial_T U.$$

Going into the co-traveling frame $U(X,T) = \phi(KX - \Omega T) = \phi(\zeta)$ and integrating once, this PDE becomes the second order ODE

$$\frac{d^2\phi}{dr^2} = B + C\phi - D\Phi'(\phi),$$

where *B* is an arbitrary integration constant and $C = 6/(K^2 \varepsilon^2)$ and $D = 6/(\Omega K \varepsilon^2)$. This suggests the trial function for the energy should be

$$\frac{v^2}{2} = A + Bu + C\frac{u^2}{2} - D\Phi(u), \tag{15}$$

which has the advantage of being much simpler than Eq. (14). In the case that the potential is a polynomial, namely $\Phi(u) = \frac{u^2}{2} + \frac{u^4}{4}$, this trial energy is almost the same as the trial energy considered in Section 3, see Eq. (7). The only difference is the missing cubic term in Eq. (15). Thus, this trial function is more restrictive, but is "derivable", and gives a physical meaning of the parameters of the fitting function in terms of wave parameters K, Ω . This is in contrast to the fit function used in Section 3, which was chosen out of the sake of simplicity. Despite the

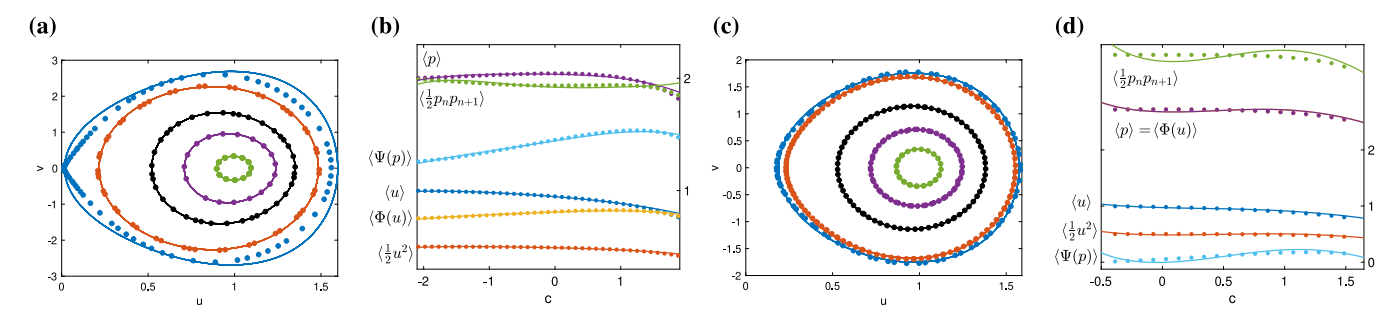


Fig. 5. (a) Same as Fig. 4, but using the regularized quasi-continuum reduction.

slightly more restrictive nature of the trial energy, the results are reasonable when comparing the ODE prediction to the full lattice DSW dynamics, see Fig. 5. In both the polynomial and KvM potential, the Rosenau-type prediction is better than the non-regularized prediction (compare Figs. 5 and 4). However, the Rosenau-type prediction is worse than the prediction based on the general 4th order polynomial energy (compare Figs. 5 and 3).

The results of the non-regularized and regularized quasicontinuum predictions suggest that the inherent underlying planar ODE structure is not due solely to the large lattice size of the problem, since the prediction based on the more generic 4th order polynomial energy leads to the best results. While further investigation of the origin and structure of the planar ODE structure of the lattice DSW lies beyond the scope of the present article, it appears to us to certainly be an issue worthy of additional attention.

5. Modulation theory

We will now briefly describe the modulation equations from the perspective of local conservation laws, and discuss the comparison thereof with the results obtained using the planar ODE reduction. For the sake of completeness, the derivation of the modulation equations in terms of the wave parameters using Whitham's method of the averaged Lagrangian is included in Appendix A.

One can derive modulation equations by averaging local conservation laws of the system [7,11]. Upon evaluation of the local averages, one can express the equations in terms of the original wave parameters, such as mean amplitude, modulation wavenumber, etc. If the equations are tractable, one solves the modulation equations in a self-similar frame subject to boundary data that are consistent with the DSW (namely that the states u_- and u_+ are connected via the modulated wave train). For a detailed discussion of this procedure see [44,56].

The equation of motion (1) implies the discrete energy law

$$\frac{d}{dt}\Phi(u_n) + \left(\frac{1}{2}\Phi'(u_n)\Phi'(u_{n+1})\right) - \left(\frac{1}{2}\Phi'(u_{n-1})\Phi'(u_n)\right) = 0,$$

and we observe that both equations are discrete counterparts of conservation laws since the time derivative of a microscopic observable equals a discrete spatial derivative of another quantity. Using the concept of weak convergence, we can pass to a continuum limit and obtain the weak formulation of the macroscopic PDE

$$\begin{array}{ll} \partial_T \langle u_n \rangle & + \partial_X \langle p_n \rangle = 0, \\ \partial_T \langle \Phi(u_n) \rangle & + \partial_X \left\langle \frac{1}{2} p_n p_{n+1} \right\rangle & = 0, \end{array} \tag{16}$$

where $p_n = \Phi'(u_n)$ and the angle-brackets denote macroscopic fields that depend on X and T. More precisely, denoting by φ a

smooth and compactly supported test function we have

$$\sum_{n} \int \frac{d}{dt} u_n(t) \, \varphi(\varepsilon n, \varepsilon t) \to - \iint \langle u_n \rangle (X, T) \, \partial_T \varphi(X, T) dX dT,$$

as $\varepsilon \to 0$ thanks to the scaling relations $T = \varepsilon t$, $X = \varepsilon n$ and integration by parts with respect to time. The field $\langle u_n \rangle$ represents the weak limit of u_n and its value at any point (X,T) can be viewed as the mean value of $u_n(t)$ in a mesoscopic space–time window centered around that point. Similar arguments apply to discrete spatial derivatives and to other observables, so (16) is an immediate consequence of the lattice dynamics. For a space–time continuous conservation law system, translation invariance yields another conservation law (momentum) via Noether's theorem. Following this naively for the lattice system, one finds the equation

$$\partial_T \left\langle \frac{1}{2} u^2 \right\rangle + \partial_X \left\langle \Psi(p) \right\rangle = 0,$$

where $\Psi(p) = pu - \Phi(u)$ is the Legendre transform of $\Phi(u)$. In the lattice setting, however, there is no translation invariance, and hence, no corresponding conserved quantity. For this reason, one cannot expect this third modulation equation to be valid in the lattice setting and, thus, the set of modulation equations is incomplete. A complete set of three modulation equations is discussed in Appendix A. Since our goal is not to use modulation equations to obtain a description of the DSWs (although we recognize that the latter is the standard approach towards their description to which we offer an alternative herein), the missing modulation equation is not critical to our discussion. Indeed, the proposed ODE reduction approach allows us to avoid the modulation equations entirely, and they are presented here only to demonstrate that our ODE reduction is consistent with the modulation theory.

We claimed the modulation Eqs. (16) are valid in the lattice setting, a feature that we now further discuss. A DSW will have a self-similar structure and thus, it is useful to define the self-similar coordinate c=X/T in which case the modulation equations become

$$\frac{d}{dc}\langle p_n \rangle = c \frac{d}{dc}\langle u_n \rangle,\tag{17}$$

$$\frac{d}{dc}\left(\frac{1}{2}p_np_{n+1}\right) = c\frac{d}{dc}\langle\Phi(u_n)\rangle. \tag{18}$$

The first modulation equation is inspected by plotting the quantities $\frac{\mathrm{d}}{\mathrm{d}c}\langle p_n\rangle$ and $c\frac{\mathrm{d}}{\mathrm{d}c}\langle u_n\rangle$ as functions of c, see the blue lines and markers of Fig. 6(a), where overlapping curves correspond to the modulation equation being valid. The validity of the second modulation equation is demonstrated in Fig. 6(b), where the quantities $\frac{\mathrm{d}}{\mathrm{d}c}\langle p_n p_{n+1}/2\rangle$ and $c\frac{\mathrm{d}}{\mathrm{d}c}\langle \Phi(u_n)\rangle$ are shown as functions of c, see the blue lines and markers of Fig. 6(b). The ODE predictions of these quantities are consistent with the modulation equations for regions sufficiently far from the leading edge of the DSW,

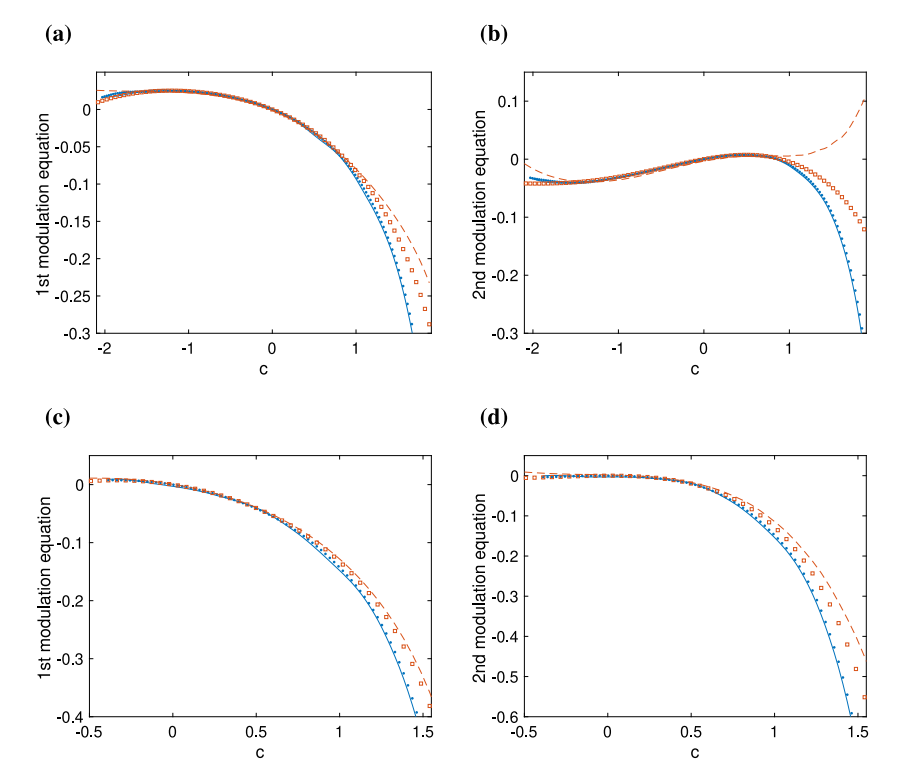


Fig. 6. Top row: Comparison of ODE predictions and full lattice DSW dynamics for the polynomial potential $\Phi(u) = u^2/2 + u^4/4$. (a) Plot of the quantity $\frac{d}{dc}\langle p_n\rangle$ for the lattice DSW (blue solid line) and the ODE prediction (red dashed line). Plot of the quantity $c\frac{d}{dc}\langle u_n\rangle$ for the lattice DSW (blue points) and the ODE prediction (red squares). (b) Plot of the quantity $\frac{d}{dc}\langle p_np_{n+1}/2\rangle$ for the lattice DSW (blue solid line) and the ODE prediction (red dashed line). Plot of the quantity $c\frac{d}{dc}\langle \Phi(u_n)\rangle$ for the lattice DSW (blue points) and the ODE prediction (red squares). **Bottom row:** Same as the top row with the KvM potential $\Phi(u) = \exp(u)$.

see the red dashed lines and squares of Fig. 6(a,b). There is noticeable deviation of the ODE prediction corresponding to the second modulation equation for $c \approx 1.1$, and it is found to be larger in the case of the polynomial potential. In particular, the ODE prediction (red dashed line) becomes positive while in the full lattice dynamics the relevant quantity is negative. This large deviation stems from small deviations of $\langle p_n p_{n+1}/2 \rangle$ due to changes in slope. In particular, in Fig. 3(a) note how the ODE prediction (green line) is increasing, whereas, the actual lattice DSW quantity (green markers) is decreasing. This observation is consistent with general deviations of the ODE orbits and full lattice DSW orbits at the edges of the DSW discussed previously, with the deviations in terms of derivatives of the local averages being more noticeable. Overall, however, Fig. 6 demonstrates that the ODE reduction is consistent with the modulation equations for regions of the DSW sufficiently far from the leading and trailing edges. The results for the KvM potential are similar and even slightly better, see Fig. 6(c,d). Note that the second modulation equation is also consistent with the ODE prediction, even for wave speeds close to the leading edge, as shown in Fig. 6(d).

6. Conclusions & future challenges

In the present work, we have demonstrated that there is an underlying low-dimensional structure within the core of a lattice DSW. The standard approach based on Whitham modulation theory is for most purposes impractical in the context of lattice DSWs. For this reason, we have argued about the relevance of elucidating and identifying either via a data-driven or in an approximate (quasi-continuum) analytical way the form of this effective planar ODE description of the lattice DSWs. We have argued that this approach can yield the kind of information typically inferred from the modulation equations, but it is much simpler in its implementation, given that it only requires the

analysis of a planar ODE. Indeed, in principle, our data-driven approach, which has proved most efficient in the numerical examples considered herein, only needs a suitable manipulation of the data set stemming from a (e.g., potentially black-box) integrator in order to be set up. We believe that the present findings may help lay the groundwork for further studies that adopt such a low-dimensional approach towards the study of lattice DSWs as an alternative to modulation theory, including in a variety of different models (such as, e.g., in discrete models of the nonlinear Schrödinger variety [38,57,58]). For example, we showed that the most natural candidate for the underlying ODE based on the quasi-continuum approach did not perform as well as the simple polynomial approximation. We also considered an alternative variant via the Rosenau regularization which was deemed to be more effective than the former but less so than the latter (yet was also systematically possible to obtain from the microscopic model). The different approaches suggest there may be other derivable ODEs waiting to be discovered and exploited in a manner similar to that presented here. Other techniques, such as the DSW fitting method detailed in [11], could also be applied to this lattice (since the dispersion relation is known explicitly) and would be of particular interest to consider. On a broader (and more challenging) scale, a potential self-consistent, general formulation of the Whitham modulation equations for nonlinear dynamical lattices remains an important, but highly challenging task as was highlighted herein. Arguably, this is, to a nontrivial degree, due to the lack of some symmetries (most notably of translation invariance) in the lattice setting. Studies along these directions are currently underway and will be reported in future publications.

CRediT authorship contribution statement

Christopher Chong: Methodology, Formal analysis, Writing – original draft. **Michael Herrmann:** Conceptualization, Formal

analysis, Writing – review & editing. **P.G. Kevrekidis:** Validation, Formal analysis, Writing – review & editing.

Declaration of competing interest

The authors declare that they have no known competing financial interests or personal relationships that could have appeared to influence the work reported in this paper.

Acknowledgments

The present paper is based on work that was supported by the US National Science Foundation under Grant No. DMS-2107945 (CC) and DMS-1809074, as well as DMS-2204702 (PGK).

Appendix A. Modulation equations in terms of wave parameters

For the sake of completeness, we present the modulation equations in terms of the wave parameters using Whitham's method of the averaged Lagrangian. For the lattice, this procedure yields a complete set of three modulation equations, but, as the derivation will demonstrate, working with them is cumbersome.

The formal procedure to obtain Whitham modulation equations in the lattice setting is well-known [28,29]. Although rigorous error estimates in lattice or continuous settings are rare (see [29,59] for special examples), numerical simulations do suggest they are valid [60]. Before writing the modulation equations, we must re-write the traveling wave equation – and actually also the lattice – using an integral formulation. We start by recalling that traveling periodic waves of Eq. (1) have the form $u_n(t) = V + \mathcal{V}(\zeta)$, $\zeta = Kn - \Omega t$, where the parameters V (mean), K (wavevector) and Ω (frequency) are real and the wave profile \mathcal{V} is assumed, w.l.o.g, to be 2π periodic with mean zero. The traveling wave equation has a variational structure, which will be exploited to derive modulation equations. To see this, we define the centered difference operator ∇_K (which is skew-symmetric) by

$$(\nabla_K \mathcal{F})(\zeta) = \mathcal{F}(\zeta + K) - \mathcal{F}(\zeta - K),$$

and define ${\cal W}$ via

$$V = \nabla_K W. \tag{A.1}$$

Note that the traveling wave Eq. (6) is just the Euler-Lagrange equation

$$\partial_{\mathcal{W}} \mathcal{L}(\mathcal{W}, V, K, \Omega) = 0,$$

to the Lagrangian functional

$$\mathcal{L}(\mathcal{W}, V, K, \Omega) = \Omega \mathcal{S}(\mathcal{W}, K) - \mathcal{E}(\mathcal{W}, V, K), \tag{A.2}$$

where

$$S(W, K) = \frac{1}{2\pi} \int_{0}^{2\pi} (\nabla_{K} W)(\zeta) \cdot W'(\zeta) d\zeta, \qquad (A.3)$$

and

$$\mathcal{E}(\mathcal{W}, V, K) = \frac{1}{2\pi} \int_{0}^{2\pi} \Phi\left(V + (\nabla_{K} \mathcal{W})(\zeta)\right) d\zeta. \tag{A.4}$$

The traveling wave equation can then be written as

$$\Omega \, \partial_{\mathcal{W}} \mathcal{S} (\mathcal{W}, K) = \partial_{\mathcal{W}} \mathcal{E} (\mathcal{W}, V, K) \,, \tag{A.5}$$

where Ω plays the role of a Lagrange multiplier. For the linear model, Ω is related to K through the dispersion relationship, but for nonlinear functions Φ' , we expect that V, K and Ω are independent parameters. The existence of a three-parameter family of traveling wave solutions to Eq. (1) was demonstrated in [35],

albeit with different parameters and using a certain reformulation of (6).

The DSW can be thought of as a traveling wave, as just described, but now the wave parameters V, K and Ω vary in time and space. This motivates an ansatz for an approximate modulated wave solution,

$$w_n(t) \approx \frac{1}{2\varepsilon} A(X,T) + \mathcal{W}\left(X,T; \frac{1}{\varepsilon} Z(X,T)\right),$$
 (A.6)

where the modulated traveling waves parameters are given by

$$V = \partial_X A$$
, $\Omega = -\partial_T Z$, $K = \partial_X Z$.

If one substitutes ansatz (A.6) into the total action integral for Eq. (1), that is

total action
$$= -\int \sum_{n} \dot{w}_{n}(t) \big(w_{n+1}(t) - w_{n-1}(t) \big) dt$$
$$-\int \sum_{n} \Phi \big(w_{n+1}(t) - w_{n-1}(t) \big) dt ,$$

and replaces summation by integrals, one arrives at the expression:

total action =
$$-\frac{1}{2} \int_0^{T_f} \int_{X_0}^{X_f} \partial_T A \, \partial_X A \, dT dX$$

 $+ \int_0^{T_f} \int_{X_0}^{X_f} L_{\text{TW}}(\partial_X A, \partial_X Z, -\partial_T Z) \, dT dX$,

where

$$L_{\text{TW}}(V, K, \Omega) = \mathcal{L}(\mathcal{W}_*(V, K, \Omega), V, K, \Omega), \tag{A.7}$$

is the action function for lattice traveling waves and \mathcal{W}_* stands for a solution to (A.5). The variations with respect to A and Z provide the two equations

$$\partial_T V - \partial_X \partial_V L_{TW} = 0,
\partial_T \partial_C L_{TW} - \partial_X \partial_K L_{TW} = 0,$$
(A.8)

which provide in combination with the integrability (the socalled "conservation of waves") condition

$$\partial_T K + \partial_X \Omega = 0, \tag{A.9}$$

the three modulation equations with respect to the variational parameter set V, K, and Ω . Setting $S=\partial_{\Omega}L_{\text{TW}}$ and regarding the Legendre transform

$$E_{\text{TW}} = S \Omega - L_{\text{TW}}, \tag{A.10}$$

as a function in V, S, and Ω , the macroscopic parameter dynamics can equivalently be written as

$$\partial_T V + \partial_X \partial_V E = 0,
\partial_T K + \partial_X \partial_S E = 0,
\partial_T S + \partial_X \partial_K E = 0.$$
(A.11)

This is a system of three nonlinear conservation laws in which the densities completely determine the fluxes. The corresponding constitutive relations are all encoded in the equation of state (A.10), which depends via

$$E_{\text{TW}}(V, K, S) = \mathcal{E}(\mathcal{W}_*(V, K, S), V, K), \tag{A.12}$$

on the three-dimensional family of lattice waves, where \mathcal{W}_* now denotes a traveling wave with parameters V, K, and S, that is a critical point of the energy functional (A.4) subject to the constraint $S(\mathcal{W}_*, K) = S$ as in (A.3). By means of the reformulation

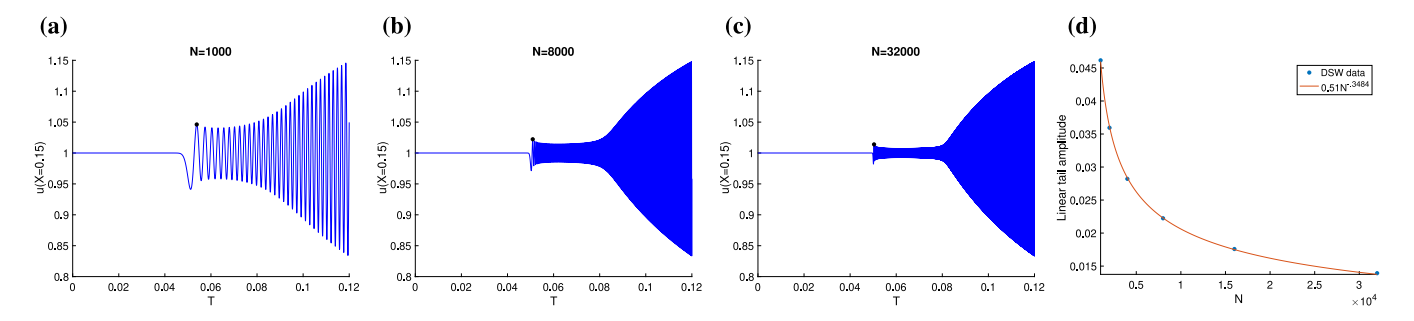
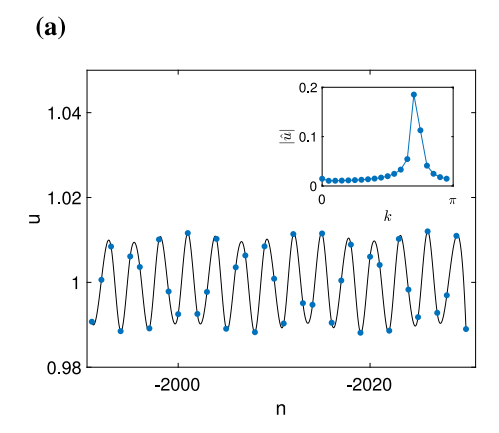


Fig. 7. Time series data for fixed X = 0.15 for the lattice sizes (a) N = 1000, (b) N = 8000 and (c) $N = 32\,000$. The black dot is taken as the reference point to measure the amplitude of the linear wave (first local maximum of the linear wave). (d) Plot of the amplitude of the linear wave (i.e. the black points) against the lattice size N. The red curve is the best-fit curve of the form aN^b , where a = 0.51 and b = -0.3484, which is consistent with the linear theoretical prediction that the decay law is $\sim N^{-1/3}$.



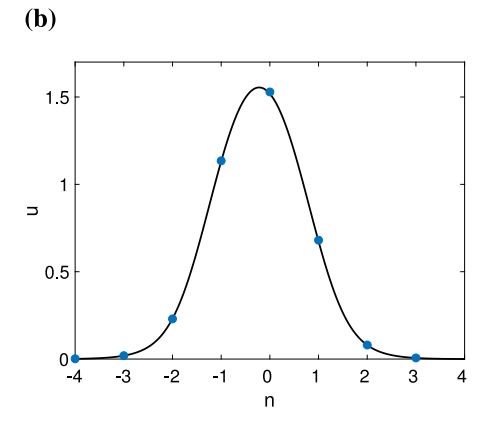


Fig. 8. (a) Spatial profile of the DSW shown in Fig. 1(a) near the trailing edge (markers). The solid curves are the interpolating cubic-splines. The inset shows the magnitude of the Fourier transform, which is spectrally concentrated near the wavenumber $k \approx 2.2$. **(b)** Numerical solitary wave solution of Eq. (6) (solid curve) and leading edge of the lattice DSW shown in Fig. 1(a) (markers).

(A.11), one readily verifies that the modulation Eqs. (A.11) are of Hamiltonian type and imply (at least for smooth solutions) a fourth conservation law, namely

$$\partial_T E_{\text{TW}} + \partial_X \left(\frac{1}{2} \left(\partial_V E_{\text{TW}}\right)^2 + \partial_K E_{\text{TW}} \partial_S E_{\text{TW}}\right) = 0. \tag{A.13}$$

The Whitham approach, therefore, predicts four macroscopic conservation laws to be valid within each DSW with only three of them being independent. The first equation in (A.11) and the extension PDE (A.13) correspond to the two equations in (16) and, therefore, possess an immediate microscopic interpretation. The second equation in (A.11) is just the consistency relation (A.9) between the wave number K and the frequency $\Omega = \partial_S E_{TW}$, but due to the nonlinear nature of the underlying lattice waves, it is

very hard to relate these quantities to local space–time averages of microscopic observables. For the conservation law with density *S*, we likewise miss an interpretation on the particle scale. For PDE models, this equation links to the conserved quantity that stems from the shift invariance according to the Noether theorem, but its microscopic meaning remains unclear in the context of lattices and other particle systems. This is arguably even more so in light of our earlier discussion about the absence of translational invariance in the latter context.

Despite the elegance of Whitham's variational approach to modulation theory, very little is known about the analytical properties of $E_{\rm TW}$ and its derivatives. Except for integrable or very degenerate cases, it is not even clear whether (A.11) is really a hyperbolic PDE and how to characterize or compute the self-similar rarefaction waves that correspond to the DSW. This lack of qualitative (and even more so, quantitative) information was one of the main motivations for following the alternative data-driven approach described in the main text.

A particular difficulty in the nonintegrable lattice setting is the dependence of the wave profile on an advance-delay differential equation. Even the numerical simulation of the modulation equations can be quite cumbersome, as discussed in [60]. While the analysis of the modulation equations from this perspective is certainly interesting and important, it is, as discussed above, beyond the scope of the present article.

Appendix B. Inspection of trailing and leading edge

In the main text, we showed the ODE reduction was reasonable within the core of the DSW. In this appendix, we briefly inspect the trailing and leading edge of the DSW.

According to the linear theory, the amplitude of the linear wave at the trailing edge of the DSW can be shown to follow the decay law $\sim N^{-1/3}$ with the use of Fourier analysis [43]. In Fig. 7, time series plots are shown for three lattice sizes, N=1000, N=8000 and $N=32\,000$ where it is seen that the amplitude of linear waves is decreasing. In particular, the time series for the X=0.15 node is shown, where $X=\varepsilon n$ and $\varepsilon=1/N$. In these graphs, the slow variable is defined as $T=\varepsilon t$. The last panel shows a plot the amplitude of the linear wave against the lattice size N where it is seen that the observed decay is consistent with the theoretical decay law $\sim N^{-1/3}$.

We expect that the local behavior of the tail can be described by small amplitude waves. They should comply with the dispersion relation

$$\Omega = \Phi''(V_*) \sin(K),$$

where V_* represents the constant state behind the wave and can be regarded as independent of c (at least to leading order). Modulation Eq. (A.9) implies

$$\frac{\mathrm{d}}{\mathrm{d}c}\Omega\left(c\right)=c\,\frac{\mathrm{d}}{\mathrm{d}c}K\left(c\right)\qquad\text{for}\quad c\gtrapprox c_{-},$$

where c_{-} denotes the speed of the trailing edge. We thus obtain the simplified law

$$c = \frac{\mathrm{d}\Omega}{\mathrm{d}K} = \Phi''(V_*)\cos(K(c)) \quad \text{for } c \gtrsim c_-,$$
 (B.1)

This formula allows one, in principle, to predict the wave speed via knowledge of the wavenumber. We estimate the wave number near the trailing edge of the DSW shown in Fig. 1(a) by computing the Fourier transform $\hat{u}(k)$ of the spatial profile in a small window near n=-2000 after subtracting the constant background state. The spectral peak provides an estimate for the wavenumber, see Fig. 8(a). We found that $k\approx 2.2$, which according to Eq. (B.1) corresponds to $c\approx -2.35$. This is reasonably close to the numerically estimated trailing edge speed of $c_-=-2.5$ reported earlier in the text.

The local behavior at the leading edge of the DSW should be described by a solitary wave, since the wavenumber approaches zero as the leading edge is approached. To verify this, we compute a solitary wave in the lattice by solving Eq. (6) using the fixed-point iteration routine described in [35] subject to a fixed wave speed of $c = c_+ = 2.45$ (the leading edge speed). The initial guess is given by the profile of the leading edge. The resulting numerical solitary wave solution of Eq. (6) is shown as the continuous curve in Fig. 8(b), which compares favorably to the leading edge of the lattice DSW, shown as markers.

References

- [1] H.W. Liepmann, A. Roshko, Elements of Gasdynamics, Wiley, New York, 1957
- [2] R. Courant, K.O. Friedrichs, Supersonic Flow and Shock Waves, Springer-Verlag, Berlin, 1948.
- [3] R.J. LeVeque, Finite Volume Methods for Hyperbolic Problems, Cambridge University Press, Cambridge, 2002.
- [4] J. Smoller, Shock Waves and Reaction-Diffusion Equations, Springer-Verlag, New York, 1983.
- [5] Michelle D. Maiden, Nicholas K. Lowman, Dalton V. Anderson, Marika E. Schubert, Mark A. Hoefer, Observation of dispersive shock waves, solitons, and their interactions in viscous fluid conduits, Phys. Rev. Lett. 116 (2016) 174501.
- [6] Henry Favre, Étude théorique et expérimentale des ondes de translation dans les canaux découverts, 1935.
- [7] G.B. Whitham, Linear and Nonlinear Waves, Wiley, New York, 1974.
- [8] A.V. Gurevich, L.P. Pitaevskii, Nonstationary structure of a collisionless shock wave. Zhurnal Eksp. I Teoret, Fiz. 65 (1973) 590–604.
- [9] V. Karpman, Nonlinear Waves in Dispersive Media, Pergamon Press, New York, 1975.
- [10] G.A. El, M.A. Hoefer, M. Shearer, Dispersive and diffusive-dispersive shock waves for nonconvex conservation laws, SIAM Rev. 59 (2017) 3.
- [11] G.A. El, M.A. Hoefer, Dispersive shock waves and modulation theory, Physica D 333 (2016) 11.
- [12] M.A. Hoefer, M.J. Ablowitz, I. Coddington, E.A. Cornell, P. Engels, V. Schweikhard, Dispersive and classical shock waves in Bose-Einstein condensates and gas dynamics, Phys. Rev. A 74 (2006) 023623.
- [13] R. Meppelink, S.B. Koller, J.M. Vogels, P. van der Straten, E.D. van Ooijen, N.R. Heckenberg, H. Rubinsztein-Dunlop, S.A. Haine, M.J. Davis, Observation of shock waves in a large Bose-Einstein condensate, Phys. Rev. A 80 (2009) 043606.
- [14] W. Wan, S. Jia, J.W. Fleischer, Dispersive superfluid-like shock waves in nonlinear optics, Nat. Phys. 3 (2007) 46–51.
- [15] Gang Xu, Matteo Conforti, Alexandre Kudlinski, Arnaud Mussot, Stefano Trillo, Dispersive Dam-Break flow of a photon fluid, Phys. Rev. Lett. 118 (2017) 254101.
- [16] Michelle D. Maiden, Dalton V. Anderson, Nevil A. Franco, Gennady A. El, Mark A. Hoefer, Solitonic dispersive hydrodynamics: Theory and observation, Phys. Rev. Lett. 120 (2018) 144101.
- [17] D.H. Tsai, C.W. Beckett, Shock wave propagation in cubic lattices, J. Geophys. Res. 71 (1966) 2601.
- [18] V.F. Nesterenko, Dynamics of Heterogeneous Materials, Springer-Verlag, New York, 2001.
- [19] E. Hascoet, H.J. Herrmann, Shocks in non-loaded bead chains with impurities, Eur. Phys. J. B 14 (2000) 183.
- [20] E.B. Herbold, V.F. Nesterenko, Solitary and shock waves in discrete strongly nonlinear double power-law materials, Appl. Phys. Lett. 90 (2007) 261902.

- [21] A. Molinari, C. Daraio, Stationary shocks in periodic highly nonlinear granular chains, Phys. Rev. E 80 (2009) 056602.
- [22] E.B. Herbold, V.F. Nesterenko, Shock wave structure in a strongly nonlinear lattice with viscous dissipation, Phys. Rev. E 75 (2007) 021304.
- [23] H. Kim, E. Kim, C. Chong, P.G. Kevrekidis, J. Yang, Demonstration of dispersive rarefaction shocks in hollow elliptical cylinder chains, Phys. Rev. Lett. 120 (2018) 194101.
- [24] Shu Jia, Wenjie Wan, Jason W. Fleischer, Dispersive shock waves in nonlinear arrays, Phys. Rev. Lett. 99 (2007) 223901.
- [25] G. Iooss, Travelling waves in the Fermi-Pasta-Ulam lattice, Nonlinearity 13 (2000) 849.
- [26] A. Pankov, Travelling Waves and Periodic Oscillations in Fermi-Pasta-Ulam Lattices, Imperial College Press, London, 2005.
- [27] M. Herrmann, Unimodal wavetrains and solitons in convex Fermi-Pasta-Ulam chains, Proc. R. Soc. Edinburgh: Sec. A Math. 140 (2010)
- [28] A.M. Filip, S. Venakides, Existence and modulation of traveling waves in particles chains, Comm. Pure Appl. Math. 52 (1999) 693.
- [29] W. Dreyer, M. Herrmann, A. Mielke, Micro-macro transition in the atomic chain via Whitham's modulation equation, Nonlinearity 19 (2005) 471.
- [30] A. Bloch, Y. Kodama, Dispersive regularization of the Whitham equation for the Toda lattice, SIAM J. Appl. Math. 52 (1992) 909–928.
- [31] S. Venakides, P. Deift, O. Roger, The toda shock problem, Comm. Pure Appl. Math. 44 (1991) 1171.
- [32] B.L. Holian, H. Flaschka, D.W. McLaughlin, Shock waves in the Toda lattice: Analysis, Phys. Rev. A 24 (1981) 2595.
- [33] M.J. Ablowitz, M. Hoefer, Dispersive shock waves, Scholarpedia 4 (2009)
- [34] C.V. Turner, R.R. Rosales, The small dispersion limit for a nonlinear semidiscrete system of equations, Stud. Appl. Math. 99 (1997) 205.
- [35] Michael Herrmann, Oscillatory waves in discrete scalar conservation laws, Math. Models Methods Appl. Sci. 22 (2012) 1150002.
- [36] E. Fermi, J. Pasta, S. Ulam, Studies of Nonlinear Problems. I, Tech. Rep., Los Alamos National Laboratory, Los Alamos, NM, USA, 1955, pp. LA–1940.
- [37] G. Gallavotti, The Fermi-Pasta-Ulam Problem: A Status Report, Springer-Verlag, Berlin, Germany, 2008.
- [38] P.G. Kevrekidis, The Discrete Nonlinear SchrÖDinger Equation: Mathematical Analysis, Numerical Computations and Physical Perspectives, Springer, New York, 2009.
- [39] J. Cuevas, P.G. Kevrekidis, F.L. Williams, the Sine-Gordon Model and Its Applications: From Pendula and Josephson Junctions to Gravity and High Energy Physics, Springer-Verlag, Heidelberg, 2014.
- [40] Gerald Beresford Whitham, Exact solutions for a discrete system arising in traffic flow, Proc. R. Soc. Lond. Ser. A Math. Phys. Eng. Sci. 428 (1990) 49–69.
- [41] Peter D. Lax, On dispersive difference schemes, Physica D 18 (1986) 250–254.
- [42] M. Kac, Pierre van Moerbeke, On an explicitly soluble system of nonlinear differential equations related to certain Toda lattices, Adv. Math. 16 (1975) 160-169
- [43] Mielke Alexander, Patz Carsten, Uniform asymptotic expansions for the fundamental solution of infinite harmonic chains, Z. Anal. Anwend. 36 (2017) 437–475.
- [44] A.M. Kamchatnov, Nonlinear Periodic Waves and their Modulations, World Scientific, 2000.
- [45] Eugene Kogan, The kinks, the solitons and the shocks in series-connected discrete josephson transmission lines, Phys. Status Solidi (B) (2022) 2200160.
- [46] Prashant K. Purohit, Rohan Abeyaratne, On the dissipation at a shock wave in an elastic bar, Int. J. Solids Struct. (2021) 111371, https://www. sciencedirect.com/science/article/pii/S0020768321004406.
- [47] C. Chong, P.G. Kevrekidis, G. Schneider, Justification of leading order quasicontinuum approximations of strongly nonlinear lattices, Disc. Cont. Dyn. Sys. A 34 (2014) 3403.
- [48] G. Schneider, H. Uecker, Nonlinear PDEs: A Dynamical Systems Approach, in: Graduate Studies in Mathematics, American Mathematical Society, 2017.
- [49] Karsten Ahnert, Arkady Pikovsky, Compactons and chaos in strongly nonlinear lattices, Phys. Rev. E 79 (2009) 026209.
- [50] Christopher Chong, Panayotis G. Kevrekidis, Coherent Structures in Granular Crystals: From Experiment and Modelling to Computation and Mathematical Analysis, Springer, New York, 2018.
- [51] Michael A. Collins, A quasicontinuum approximation for solitons in an atomic chain, Chem. Phys. Lett. 77 (1981) 342.
- [52] D. Hochstrasser, F.G. Mertens, H. Büttner, An iterative method for the calculation of narrow solitary excitations on atomic chains, Physica D 35 (1989) 259.
- [53] J.A.D. Wattis, Approximations to solitary waves on lattices. II. Quasicontinuum methods for fast and slow waves, J. Phys. A: Math. Gen. 26 (1993) 1193.

- [54] P. Rosenau, Hamiltonian dynamics of dense chains and lattices: Or how to correct the continuum, Phys. Lett. A 311 (2003) 39.
- [55] P. Rosenau, Dynamics of nonlinear mass-spring chains near the continuum limit, Phys. Lett. A 118 (1986) 222.
- [56] A.V. Gurevich, A.L. Krylov, Dissipationless shock waves in media with positive dispersion, J. Exp. Theor. Phys. 65 (1987) 943–953.
- [57] A.M. Kamchatnov, A. Spire, V.V. Konotop, On dissipationless shock waves in a discrete nonlinear Schrödinger equation, J. Phys. A: Math. Gen. 37 (2004) 5547–5568.
- [58] M.H. Hays, C.D. Levermore, P.D. Miller, Macroscopic lattice dynamics, Physica D 79 (1994) 1–15, https://www.sciencedirect.com/science/article/ pii/0167278994900353.
- [59] Wolf-Patrick Düll, Guido Schneider, Validity of Whitham's equations for the modulation of periodic traveling waves in the NLS equation, J. NonLinear Sci. 19 (2009) 453–466.
- [60] W. Dreyer, M. Herrmann, Numerical experiments on the modulation theory for the nonlinear atomic chain, Physica D 237 (2008) 255.